

See discussions, stats, and author profiles for this publication at: <https://www.researchgate.net/publication/327587053>

Response of microstructure to annealing in in situ Cu–Nb microcomposite

Article in *Journal of Materials Science* - September 2018

DOI: 10.1007/s10853-018-2865-4

CITATIONS

0

READS

69

7 authors, including:



Liping Deng

Fuzhou University

10 PUBLICATIONS 36 CITATIONS

[SEE PROFILE](#)



Bingshu Wang

Fuzhou University

16 PUBLICATIONS 241 CITATIONS

[SEE PROFILE](#)



Ke Han

Florida State University

189 PUBLICATIONS 2,090 CITATIONS

[SEE PROFILE](#)



Rongmei Niu

National High Magnetic Field Laboratory

28 PUBLICATIONS 190 CITATIONS

[SEE PROFILE](#)

Some of the authors of this publication are also working on these related projects:



National Natural Science Foundation of China [View project](#)



high magnetic field [View project](#)



Response of microstructure to annealing in in situ Cu–Nb microcomposite

Liping Deng^{1,*}, Bingshu Wang¹, Ke Han^{2,*}, Rongmei Niu², Hongliang Xiang¹, Karl T. Hartwig³, and Xiaofang Yang⁴

¹School of Mechanical Engineering and Automation, Fuzhou University, Fuzhou 350116, China

²National High Magnetic Field Laboratory, Tallahassee, FL 32310, USA

³Texas A&M University, College Station, TX 77843, USA

⁴College of Materials Science and Engineering, Chongqing University, Chongqing 400044, China

Received: 11 April 2018

Accepted: 27 August 2018

Published online:

11 September 2018

© Springer Science+Business Media, LLC, part of Springer Nature 2018

ABSTRACT

In this paper, the shape instabilities of Nb in in situ Cu–Nb microcomposite wires after exposed to different annealing treatments have been analyzed using scanning electron microscopy and transmission electron microscopy technologies. The results suggest that the thermal stability is related to misorientation among the adjacent grains at the triple joint. Most of the triple joints are composed of low-angle grain boundaries in Nb ribbons and Cu–Nb interfaces of $(111)_{\text{Cu}}// (011)_{\text{Nb}}$. These triple joints provide dragging force to interface motion so that neither the grains nor the interface boundaries show substantial changes below 500 °C. Above 500 °C, the Nb ribbons start to dissociate at the triple joints within Nb phase due to the stored energy by misorientation/distortion in Nb. Grooves and pits formed at these regions tend to promote the spheroidization of the Nb phase. Such results may enrich the studies on the microstructure evolution of Cu-based microcomposite.

Introduction

Cu–Nb microcomposite wires are of particular interest for their good combination of electrical and thermal conductivity, and magnetic and mechanical properties, which makes them excellent candidates for the generation of high magnetic fields (> 80 T) [1–3]. The microstructure and properties of Cu–Nb microcomposites at room temperature have been widely investigated [4–8]. During either the service or fabrication process, the wire may be exposed to

elevated temperatures and can suffer from Joule heating when large electrical currents pass through the wire [1, 9]. Heat treatment is usually applied during wire fabrication to reduce the effect of cold work so that further deformation is possible. It is known that the heating process leads to metallurgical changes for metals and alloys, e.g., modification of the grain size, morphology, orientation and the dislocation density, and meanwhile, this process is also suggested to apply for a fine-grained material [10, 11]. The process where dislocation strengthening

Address correspondence to E-mail: ldeng@fzu.edu.cn; han@magnet.fsu.edu

deformation is applied followed by appropriate annealing has been utilized in many metals. These materials are expected to possess high strength with high ductility due to the nano/ultrafine structure [11–15]. And the dislocation annihilation was believed to be responsible for the weakening during deformation [10, 16–18] as well as for the hardening during the annealing or straining process [19–22]. Such processes cause changes in the microstructure of Cu–Nb composite wire. In particular, the morphology changing, mostly, spheroidization and coarsening of Nb phase can occur during annealing [5, 23–26], leading to changes in properties. For example, Mara et al. [27] reported that at temperatures of 500 °C and below, no breakdown of Nb was observed and the Hall–Petch model works, while at 600 °C and above, the mechanism for the Nb coarsening gradual transforms to confined layer slip model where the dislocation motion occurs and Nb pinch off at the triple points with the Cu maintaining a deformed morphology. And the properties change remarkably although only a few percentages of the total length of Nb phase show the pinch-off character. These changes affect the service life of the wire and, eventually, the life of a magnet, while negligible changes have been reported to in Cu–Nb microcomposites after annealing below 500 °C [28, 29] or during friction stir welding under certain parameters [30]. Therefore, the effect of heat treatment on the microstructure of Cu–Nb wires has attracted considerable attention.

Several mechanisms have been proposed to explain the microstructural changes in Cu–Nb microcomposites during annealing treatment [9, 23, 31–33]. Sandim et al. [1, 9] believe that the boundary splitting¹ is the predominant mechanism for the spheroidization of Nb during heat treatment and that a large aspect ratio of width to thickness of the Nb ribbon favors the splitting process. Misra et al. [32] and Hong et al. [33] have also stated that cylinderization and spheroidization in the Nb phase are attributed to edge spheroidization or a groove-driven instability at Cu–Nb interfaces. The interfaces are suggested to be crucial in obtaining desired microstructure and corresponding properties not only in Cu-based composites but also in some duplex steels or transformation-induced plasticity steels

¹ Boundary splitting is a process where atoms migrate away from the sub-boundaries and the phase pinches off.

[34–36]. Besides, they even contribute to unexpected twinning in the Cu phase which introduces a distinct stable interface [37]. During the cylinderization and spheroidization process, phase separation and anchor structure were observed in the nanolayered Cu–Nb systems which benefit the thermal stability a lot [27, 38]. Sharma et al. [10] identified five mechanisms for the coarsening of the Nb phase and concluded that the dominant mechanism changed with different annealing stages. Most of these mechanisms are based on the final spheroidization morphology of the Nb phase. Few works focus on the process before spheroidization. The work by Zheng et al. [39] gives a new insight on the thermal stability in high-aspect-ratio Cu–Nb nanolayered composites. Their results show that the interface faceting rather than the high-energy grain boundaries or triple junctions would induce the necking and pinch off of Nb phase, although the grooving and necking still derived from the Cu–Nb interface. On the other hand, electron backscatter diffraction (EBSD) patterns are not yet been applied thoroughly on as-deformed Cu–Nb wires due to the high stress concentration in the wire. In the present work, high-resolution orientation images obtained from EBSD are used to elucidate the orientation of the Nb phase in the as-deformed sample. Meanwhile, distinct findings concerning microstructural evolution of in situ Cu–Nb microcomposite wires after heavy deformation and different temperature annealing are reported. The results are discussed by comparing the annealing response with others' results on Cu–Nb composites as well as pure Cu and Nb to pursue a deeper understanding of the microstructural changes in Cu–Nb microcomposite wires that occurs during heat treatment.

Materials and methods

The samples used in this paper are in situ Cu–Nb microcomposite wires with diameters of 1.02 and 0.16 mm, corresponding to drawing strains of 6.4 and 10.1, respectively. The detailed procedure of sample preparation has been stated in our previous work [40]. The samples were sealed, respectively, in six quartz tubes with a vacuum of about 10^{-3} Pa, followed by annealing treatment in the center of a tubular furnace at 400–900 °C for 1 h with an interval of 100 °C. It should be mentioned that although the wires are usually applied in coiled or wrapped form

for magnetic field building, considering the large size of the magnetic bore, the stress state of the straight wires in the present work can be regarded similarly to those in final application.

Scanning electron microscope (SEM) samples were etched with a solution of 20% nitric acid in deionized water after mechanical polishing. The Cu matrix was removed and shows dark in contrast. The microstructure of the wires was investigated with a field emission gun Zeiss 1540XB SEM. Several high-magnification SEM images were used to obtain the dimensions of the Nb phase with Image-Pro Plus software, while two typical images for each sample are shown in Fig. 1. The samples for high-resolution EBSD (HR-EBSD) mapping were ground with 400–4000 grit papers followed by ion polishing, the examinations were carried out on a Zeiss Supra 55 FEG-SEM, and the data analysis was accomplished with HKL channel 5 system. Transmission electron microscope (TEM) samples were prepared by mechanical thinning followed by dimpling and ion milling on a liquid nitrogen stage. TEM observations were carried out using a JEOL 2011 TEM operated at 200 kV.

Results and discussion

Figure 1 shows SEM images of the as-drawn Cu–Nb microcomposite wires. The Nb phase (light regions in Fig. 1a, c) shows a curled shape in the cross section; the more deformation the wire undergoes, the more curling of the Nb is seen. The average radii of the Nb ribbons are measured to decrease from 46.1 to 19.7 nm for wires drawn to strain from 6.4 to 10.1, corresponding to curvatures of 0.022 nm^{-1} and 0.051 nm^{-1} . From the longitudinal section images of the wires (Fig. 1b, d), we can see that the Nb exhibits a thin ribbon shape along the length. When the wires were drawn from a strain of 6.4–10.1, the average width (w) of the Nb ribbons was reduced from 3132 ± 40 to 1036 ± 20 nm, and the average thickness (t) from 99 ± 15 to 25 ± 5 nm, resulting in an aspect ratio (w/t) increasing from 31.6 to 41.4. These ratios are much higher than that by Sandim et al. [1].

After annealing at $400 \text{ }^\circ\text{C}$, no obvious changes can be observed in the Nb ribbons. Both the edge and surface of the Nb ribbons are well defined (see the insets in Fig. 2a, c). This microstructural stability is considered to be attributed to the high-density Cu–

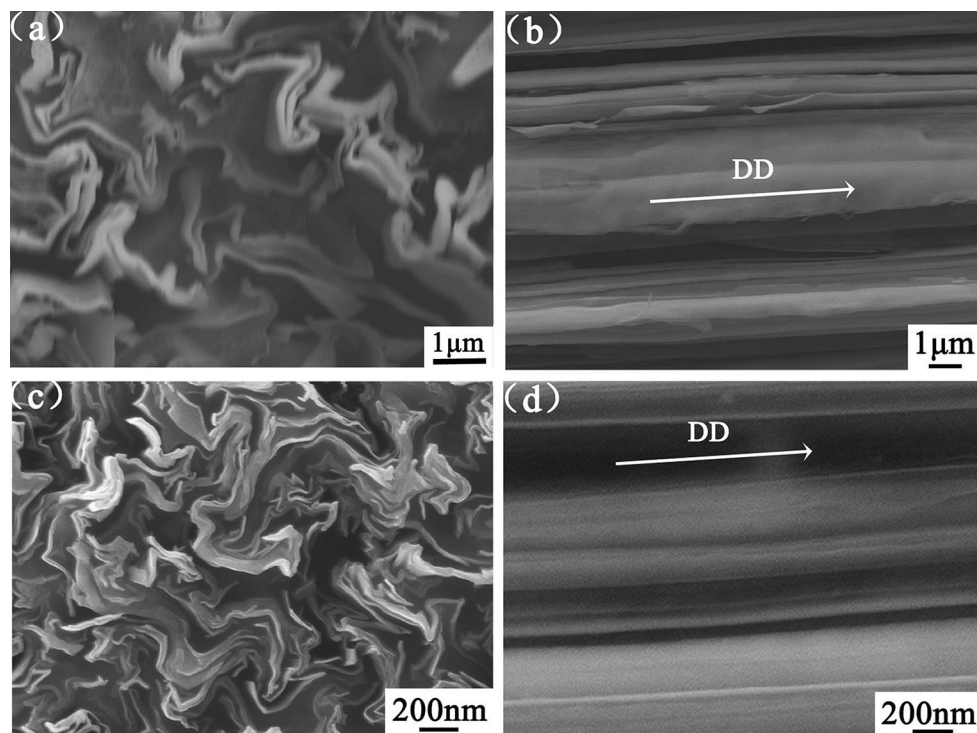


Figure 1 SEM images of Cu–Nb wires showing as-drawn microstructure at cross section (a, c) and longitudinal section (b, d): a, b, strain = 6.4; c, d, strain = 10.1. The arrows refer to the

drawing direction (DD). The dark regions are where the Cu matrix has been removed, and light regions refer to Nb phase.

Nb interfaces that arrests internal stress relaxation and delays the normal recovery and recrystallization processes, which have been found in previous works [29, 41]. The bending, folding and breakup of the Nb ribbons in Fig. 2a, c are due to the removal of the Cu matrix by acid etching and ultrasonic cleaning during sample preparation. Nb phase will groove first than Cu matrix since it possesses higher melting temperature and higher grain boundary free energy [42, 43]. Thus, after annealing at 500 °C (Fig. 2b, d), however, the Nb ribbons show significant changes. A number of grooves and pits on the Nb ribbons can be observed, as shown by the white triangles in the insets, showing a character analogous to porous films. These grooves and pits are about sub-micrometer in size, while grooves/pits in nanometer size are not observed due to the limited resolution of SEM. To be more convincing, the bright-field image of the wire with a strain of 6.4 is shown in Fig. 3 where some Nb and Cu regions are indicated. It can be seen that most of the Nb edge is straight, while in some regions, the Nb edges with a concave or concavo-convex morphology can be observed. As stated above, the Nb phase possesses a large aspect ratio (w/t) values. Thus, the Nb ribbons with concave or concavo-convex morphology are believed to present some grooves/pits in the top view. The dimensions of these grooves/pits are less than one micrometer, and some even reach nanometer level, as displayed in Fig. 3.

At higher annealing temperatures, obvious microstructural change occurs due to the enhancement of diffusion processes [44]. Some of the Nb ribbons develop into bamboo shapes and form arrays of cylinders or rods, as indicated in Fig. 2e–h. Meanwhile, some of these become spheroidized (Fig. 2e–g) and even join adjacent Nb phases to reduce the interface energy, as shown by the black triangles in Fig. 2g, h. These microstructure evolutions indicate that other than at the Cu–Nb interface boundaries as reported in others' work [29, 41, 43, 45], the shape change of Nb ribbons in our work also starts from the Nb ribbon where the Nb–Nb boundary splitting dominates. In others' work [29, 41, 43, 45], the high density of Cu–Nb interfaces, especially those twin-induced interfaces or the intersections of grain boundaries with interphase boundaries, is claimed to be responsible for the high strength and advanced thermal stability of the Cu–Nb composites. Meanwhile, boundary splitting, edge

spheroidization and direct cylinderization have been suggested to dominate the cylinderization and spheroidization phenomena and schematic models were proposed for the process of these phenomena when the Cu–Nb wires were exposed to sufficiently high temperatures [1, 8, 32, 46]. In addition, the thermal stability in pure Cu and Nb was suggested to be related to the stored energy which was considered to stem from the special grain boundaries, like nanograin boundaries or twin boundaries [47–54], while our wires show nanostructure in Nb with average thickness of 99 ± 15 nm and 25 ± 5 nm (for wires with a strain of 6.4–10.1, respectively) and no twins were found both during our SEM and TEM observation. Thus, we assume a different origin for the microstructure changes of Nb ribbons and theorize that the microstructure changes of the Nb phase start from the triple joint grain boundaries with low-angle misorientation on the Nb ribbon other than the Cu–Nb interfaces.

Representative EBSD orientation maps of the Nb phase taken from the vertical section of the 1.02 mm wire are shown in Fig. 4. The phase map (Fig. 4a) presents the Nb phase in blue and Cu matrix in red. The inverse pole figure of Cu matrix and Nb phase presents typical $\langle 111 \rangle$ and $\langle 110 \rangle$ fiber textures along the wire axis (denoted as DD) in Fig. 4b, which has been reported both in our previous and others' work [1, 40]. It should be noted that the little spread of $\langle 111 \rangle_{\text{Cu}}$ and $\langle 110 \rangle_{\text{Nb}}$ textures with respect to the DD direction is own to the stress concentration built by the deformation and the desire for the wire to reduce the interfacial energy [45]. These induce the rotation of Cu and Nb grains away from the ideal $\langle 111 \rangle$ and $\langle 110 \rangle$ directions and, consequently, the appearance of orientation variation. Figure 4c shows the colorful band constant (BC) map of Nb phase. The color presents the level of orientation variation or distortion. The redder the color, the more severe the lattice curvature, and vice versa. The black lines refer to the boundaries with misorientation $> 15^\circ$. It can be seen that almost no high-angle grain boundaries ($> 15^\circ$) can be found in Nb phase. Misorientation angle distribution with angles below 15° is exhibited in Fig. 4d. Within this angle range, the angles below 6° account for 97%. This high content of the low-angle boundaries as well as the gradient change of the color in Fig. 4c indicates a high component of dislocations and orientation variations in Nb phase, which are responsible for the crystalline

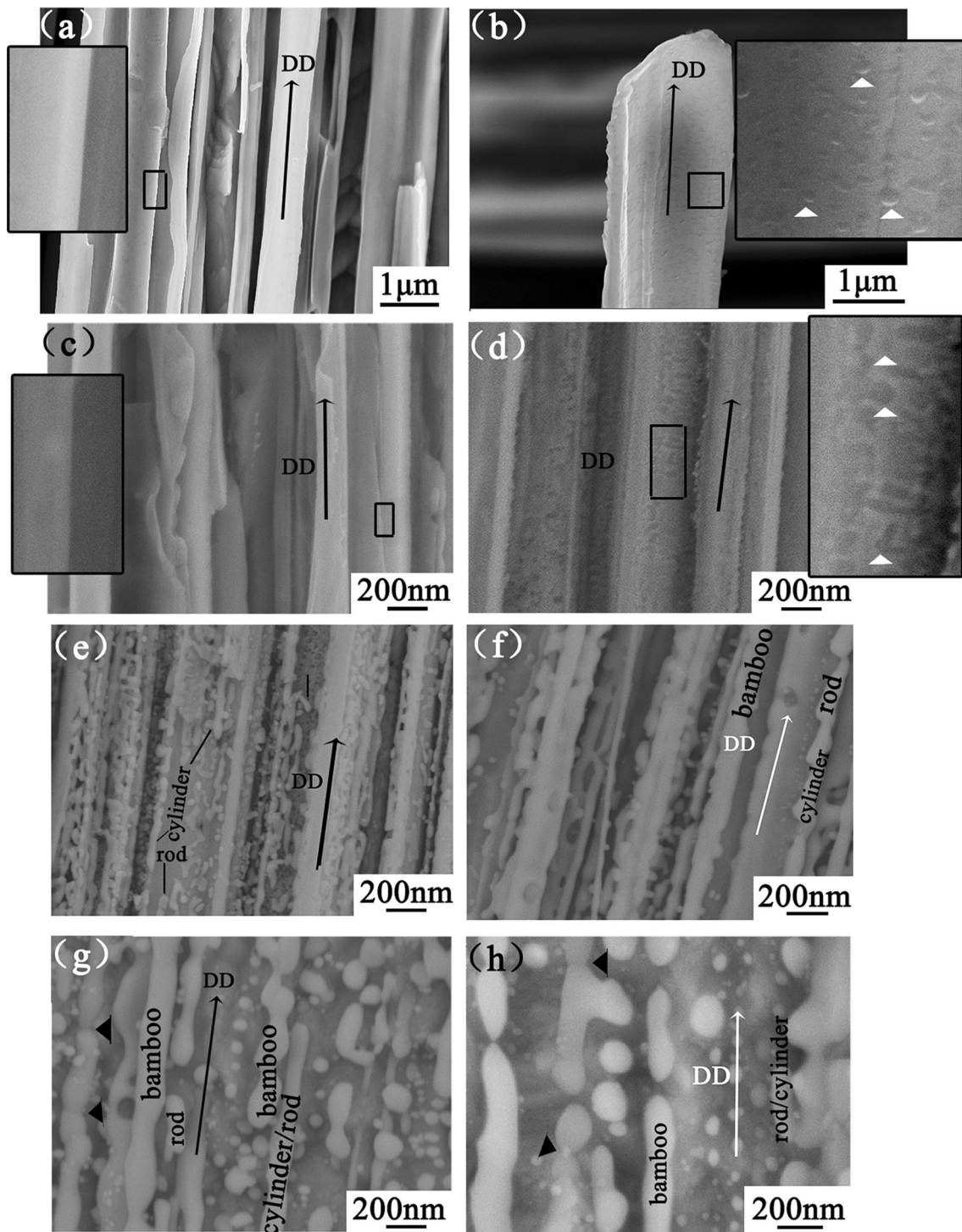


Figure 2 Longitudinal microstructure of wires after annealing at temperatures between 400 °C and 900 °C for 1 h: **a** $\eta = 6.4$, 400 °C; **b** $\eta = 6.4$, 500 °C; **c** $\eta = 10.1$, 400 °C; **d** $\eta = 10.1$, 500 °C; **e** $\eta = 10.1$, 600 °C; **f** $\eta = 10.1$, 700 °C; **g** $\eta = 10.1$,

800 °C; **h** $\eta = 10.1$, 900 °C. The arrows present the drawing direction (DD). The white triangles present the grooves/pits on Nb. The insets in **a–d** are magnified images from the rectangular regions in **a–d**, respectively.

lattice curvature or distortion [55, 56]. Several regions shown by black arrows in Fig. 4c refer to those

regions with more lattice curvature, suggesting a higher level of distortion or curvature of crystalline

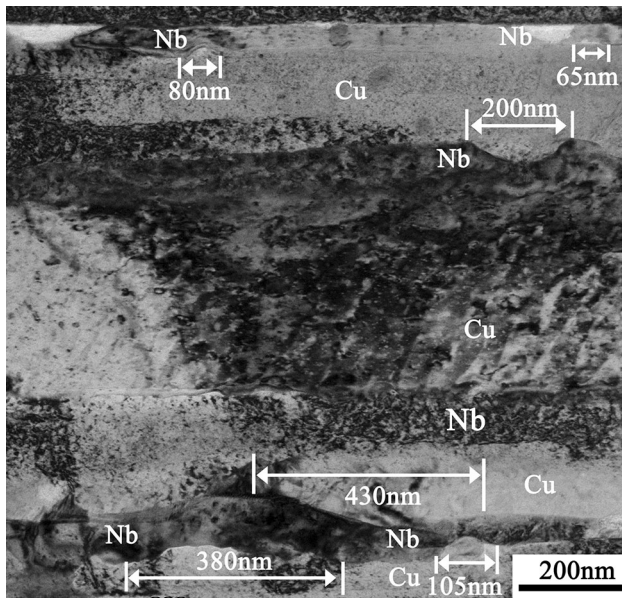


Figure 3 Bright-field image of the wire for strain $\eta = 6.4$ after annealing at 500 °C.

lattice in these regions [56, 57]. This can also be confirmed by the spread of $\langle 110 \rangle_{Nb}$ texture in Fig. 4b as well as the misorientation angle distribution of Nb phase in Fig. 4d, where the latter shows a major angle distribution range below 6°.

For more detailed observation and examination convenience, we used a TEM to examine the wire

drawn to a strain of 6.4 (1.02 mm in diameter), and the results are shown in Fig. 5. Most of the Cu–Nb interfaces show a relationship of $(111)_{Cu} // (011)_{Nb}$, which is corresponding to the EBSD results. The dark-field image (Fig. 4b) was obtained from the $(110)_{Nb}$ diffraction spot in the inset in (a); the bright part presents the Nb ribbons. These Nb ribbons show non-uniform brightness that indicates non-uniform stress and strain inside the phase even if the Nb exhibits a spheroidal shape [3]. The rich diffraction contrast suggests the presence of high internal stress which was built into the ribbons during deformation [53]. The arc of the $(110)_{Nb}$ spot is determined to be about $\pm 5.8^\circ$ with respect to the drawing direction, revealing grains with different orientations within a single ribbon. This indicates that most of the Nb ribbons are oriented to a $[110]_{Nb}$ direction within a deviation angle of $\pm 5.8^\circ$, which is corresponding to the EBSD results above and also coincident with others' work. The latter mainly suggested the deviation to be attributed to the semi-coherent Cu–Nb interfaces [58–60]. Besides, the $(110)_{Nb}$ diffraction spots display elongated circles rather than ideal round ones, and the aspect ratio of the $(110)_{Nb}$ spots reaches 1.8, which is far from the ideal value 1.0. This shape distortion is attributed to the strain field and disorder in the phase [61]. These misorientations or distortion induced by deformation can serve as stress

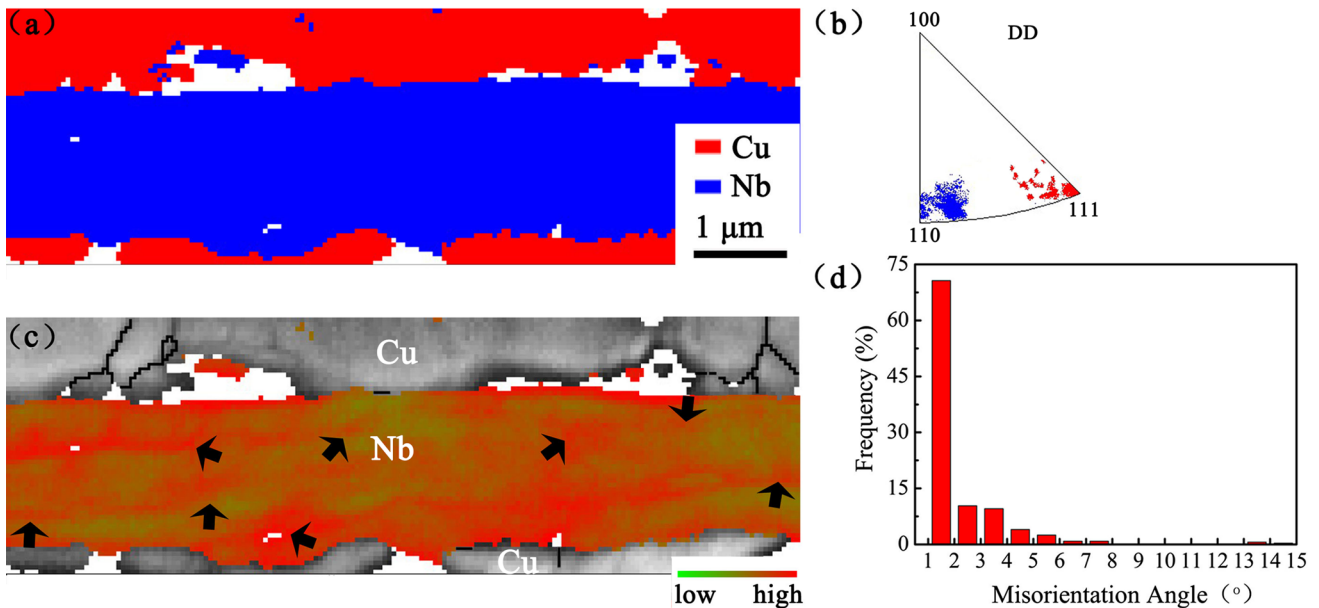


Figure 4 EBSD maps of the 1.02 mm sample. **a** phase map; **b** inverse pole figure of Nb and Cu, DD refers to drawing direction (wire axis); **c** colorful band contrast (BC) map of NB phase;

boundaries with misorientation $> 15^\circ$ are presented in black lines; **d** misorientation angle distribution in Nb phase with angle $< 15^\circ$.

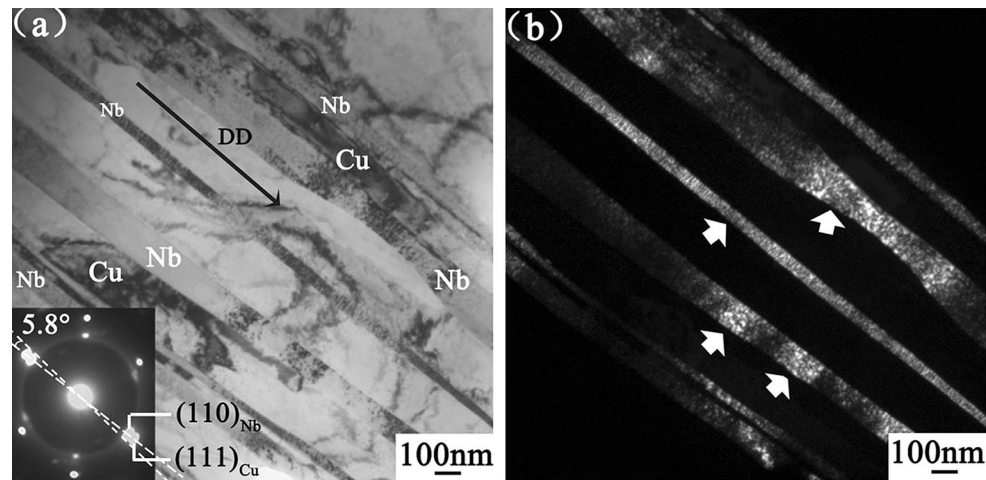


Figure 5 Longitudinal section TEM images of as-drawn wire with $\eta = 6.4$. **a** bright-field image and corresponding selected area diffraction pattern (SADP); **b** dark-field image from $(110)_{\text{Nb}}$

diffraction spot indexed in the inset in **a**. The white arrows indicate the defect regions.

sources and divide the Nb ribbons into cylinder, rod and bamboo shapes [62, 63]. In other words, the thin Nb ribbons in this work present certain misorientation or distortion with high internal stress which can provide a driving force for the recovery and recrystallization of Nb [64, 65].

Considering the comparable scale of the grooves/pits in Figs. 2b and 3, the regions with lattice distortion or curvature indicated by black arrows in Fig. 4c and the regions indicated by the white arrows in Fig. 5b, it is likely that within Nb phase the atoms start to diffuse along the triple joint of Nb low grain boundaries at misoriented regions ($\leq 5.8^\circ$, shown in the inset in Fig. 5a and white arrows in Fig. 5b). At these joints, the elastic energy resulting from the stress obtained by severe deformation is relatively high and this stress may be concentrated at the triple joints. The local peaked elastic energy encourages the diffusion of Nb atoms from these joints to the regions off the triple joint boundaries, leading to forming of irregular interfaces and moving of triple joints into misorient-concentrated Nb ribbons. To a certain degree, this is analogous to the results in pure Cu or Nb [47–54] although the latter are with high-angle misorientations, while, in Zheng et al.'s work [39] such moving phenomenon was not reported due to the single-grain layer structure. In the present work, after removal of Cu by etching, Nb ribbons show grooves and pits. These grooves and pit regions join adjacent ones or grow further to release internal stress and stored energy at high temperatures,

resulting in a bamboo-shaped Nb architecture (Fig. 2e, f). In addition, the curvature of the Nb ribbon itself is believed to provide a driving force of several MPa for Nb atoms to migrate and coalesce toward the center of the curvature [64, 66]. Thus, cylinderization and spheroidization occur to the Nb ribbons. Besides, the stored energy gradient within Nb ribbon can induce atom migration, promoting the cylinderization and spheroidization of the Nb phase [10, 67].

Model proposed

Based on the observed microstructure and the results analyzed above, the microstructural changes in Cu–Nb wire can be described as shown in Fig. 6.

The Nb ribbon is considered as a finite thin ribbon with $\pm 5.8^\circ$ deviation angle to the $[110]_{\text{Nb}}$ direction, as stated earlier. At the initial stage, the stored energy at Nb grain boundaries with the low angle ($\leq 5.8^\circ$) is relatively high as a result of severe plastic deformation (Fig. 6a). The stored energy, in turn, results in the formation of low-angle grain boundaries and triple joints. Among these boundaries, triple joint boundaries along Cu–Nb interface with a large ratio of grain boundary energy to interface energy move rapidly at high temperatures [32, 64], and grooves and pits develop (Fig. 6b) when the temperature is sufficiently elevated to drive appreciable atomic migration at these boundaries. These grooves and pits grow to minimize the internal energy as the temperature increases (Fig. 6c). Meanwhile, Cu

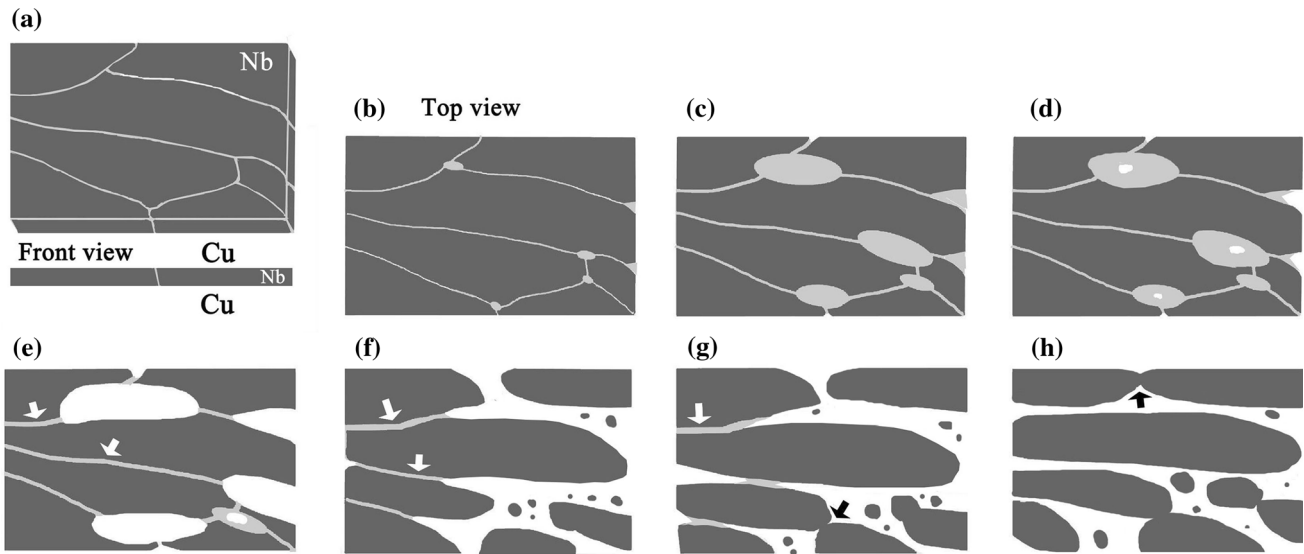


Figure 6 Model proposed. The dark regions represent the Nb phase; the gray lines and regions represent grain boundaries ($\leq 5.8^\circ$) and grooves/pits which are on the Nb ribbon; the white is vacant/holes where the Nb ribbon pinch off. **a** deformed Nb

ribbon; **b** grooves/pits form at triple joints on the Nb ribbon; **c–d** grooves/pits grow and holes form; **e–h** holes grow and join adjacent ones.

atoms diffuse along the triple joint boundaries to compensate for the geometry change at these locations [32]. As temperature increases further, the grooves become deeper, leading to pinch off at the triple point boundaries and spheroidization in Nb phase (Fig. 6d, e). Some of the grooves join adjacent ones in the same Nb ribbon (Fig. 6f). Meanwhile, concave regions (or grooves) can also come into being at the other Nb grain boundaries (as illustrated by the white arrows in Fig. 6e–g). As the Nb spheroidization and growing proceed, new concaved regions (or grooves) can be found at the locations where Nb ribbons meet, as depicted by the dark arrows in Fig. 6g and h. These concaves and grooves become deeper to minimize interface energy as annealing proceeds, resulting in cylinderization, spheroidization and islands of Nb (Fig. 6g, h) [1, 9, 31–33]. Meanwhile, some small Nb particles below 100 nm (Fig. 2g–h) can be observed. Those small particles can be related to the dissolution of Nb into Cu during wire drawing [40, 68] and nonclassic ripening effect [69]. It is suggested that the latter is related to a decrease in elastic energy, which can offset the increase in interfacial energy. Therefore, the formation of these small particles reduces the free energy and favors the microstructural and property stability of the wires. The wires with this high stability show Vickers microhardness values over 230 at

temperatures up to 500 °C [70]. From a thermal stability perspective, the composites can thus be used in various applications up to 500 °C.

Conclusions

The effect of annealing on the microstructure of Cu–Nb microcomposite wires has been investigated. The microstructure of the wires is very stable below 500 °C due to the dragging effect of the triple points, most of which are composed of low-angle grain boundaries in Nb ribbons and Cu–Nb interfaces of $(111)_{\text{Cu}}// (011)_{\text{Nb}}$. Above 500 °C or above, the low-angle misorientation within Nb ribbons with elastic energy induced by the stress at the triple joints is the principal cause for the primary shape morphology changes observed in the Nb ribbon. A schematic illustration is proposed to explain this phenomenon.

Acknowledgements

The authors greatly acknowledge the support of the National High Magnetic Field Laboratory through US National Science Foundation Cooperative Agreement No. DMR-1157490. This research is also funded by the National Natural Science Foundation of China (Grant Nos. 51601039, 51301040, 51541103), the

Danish National Research Foundation, the National Natural Science Foundation of China for Non-metals (Grant No. 51261130091), the Natural Science Foundation of Fujian Province, China (Grant No. 2016J05119), and the Collaborative Innovation Center of High-End Equipment Manufacturing in Fujian, China. Thanks are also given to Dr. Yan Xin, Dr. Yifeng Su, Dr. Xiaowei Zuo and Dr. Lei Qu for their assistance with the testing.

References

- [1] Sandim HRZ, Sandim MJR, Bernardi HH, Lins JFC, Raabe D (2004) Annealing effects on the microstructure and texture of a multifilamentary Cu–Nb composite wire. *Scr Mater* 51:1099–1104
- [2] Thilly L, Renault PO, Vidal V, Lecouturier F, Van Petegem S, Stuhr U, Van Swygenhoven H (2006) Plasticity of multiscale nanofilamentary Cu/Nb composite wires during in situ neutron diffraction: Codeformation and size effect. *Appl Phys Lett* 88:191906/191901–191906/191903
- [3] Gu T, Castelnau O, Forest S, Hervé-Luanco E, Lecouturier F, Proudhon H, Thilly L (2017) Multiscale modeling of the elastic behavior of architected and nanostructured Cu–Nb composite wires. *Int J Solids Struct* 121:148–162
- [4] Budiman AS, Narayanan KR, Li N, Wang J, Tamura N, Kunz M, Misra A (2015) Plasticity evolution in nanoscale Cu/Nb single-crystal multilayers as revealed by synchrotron X-ray microdiffraction. *Mater Sci Eng A* 635:6–12
- [5] Badinier G, Sinclair CW, Allain S, Bouaziz O (2014) The Bauschinger effect in drawn and annealed nanocomposite Cu–Nb wires. *Mater Sci Eng A* 597:10–19
- [6] Cui BZ, Xin Y, Han K (2007) Structure and transport properties of nanolaminate Cu–Nb composite foils by a simple fabrication route. *Scr Mater* 56:879–882
- [7] Pourrahimi S, Nayeb-Hashemi H, Foner S (1992) Strength and microstructure of powder metallurgy processed restacked Cu–Nb microcomposites. *Metall Trans A* 23A:573–586
- [8] Spitzig WA, Pelton AR, Laabs FC (1987) Characterization of the strength and microstructure of heavily cold worked Cu–Nb composites. *Acta Metall* 35:2427–2442
- [9] Sandim MJR, Sandim HRZ, Bernardi HH, Shiguo CY, das Virgens MG, Ghivelder L, Awaji S, Watanabe K et al (2005) Annealing effects on the microstructure, electrical, and magnetic properties of jelly-rolled Cu–Nb composite wires. *Supercond Sci Technol* 18:35–40
- [10] Chakkingal U, Suriadi AB, Thomson PF (1999) The development of microstructure and the influence of processing route during equal channel angular drawing of pure aluminum. *Mater Sci Eng A* 266:241–249
- [11] Chakkingal U, Suriadi AB, Thomson PF (1998) Microstructure development during equal channel angular drawing of Al at room temperature. *Scr Mater* 39(6):677–684
- [12] Okitsu Y, Takata N, Tsuji N (2009) A new route to fabricate ultrafine-grained structures in carbon steels without severe plastic deformation. *Scr Mater* 60(2):76–79
- [13] Figueiredo RB, Langdon TG (2010) Grain refinement and mechanical behavior of a magnesium alloy processed by ECAP. *J Mater Sci* 45(17):4827–4836. <https://doi.org/10.1007/s10853-010-4589-y>
- [14] Valiev RZ, Enikeev NA, Langdon TG (2011) Towards superstrength of nanostructured metals and alloys, produced by SPD. *Kovove Mater* 49(1):1–9
- [15] Zhao YH, Bingert JF, Liao XZ, Cui BZ, Han K, Sergueeva AV, Mukherjee AK, Valiev RZ et al (2006) Simultaneously increasing the ductility and strength of ultra-fine-grained pure copper. *Adv Mater* 18:2949–2953
- [16] Miyamoto H, Mimaki T, Vinogradov A, Hashimoto S (2002) Corrosion fatigue of ultra-fine grain copper fabricated by severe plastic deformation. *Ann Chim Sci Mater* 27:S197
- [17] Estrin Y, Vinogradov A (2013) Extreme grain refinement by severe plastic deformation: a wealth of challenging science. *Acta Mater* 61(3):782–817
- [18] Tahawy ME, Pereira PHR, Huang Y, Park H, Choe H, Langdon TG, Gubicza J (2018) Exceptionally high strength and good ductility in an ultrafine-grained 316L steel processed by severe plastic deformation and subsequent annealing. *Mater Lett* 214:240–242
- [19] Huang X, Hansen N, Tsuji N (2006) Hardening by annealing and softening by deformation in nanostructured metals. *Science* 312:249–251
- [20] Mavlyutov AM, Latynina TA, Murashkin MY, Valiev RZ, Orlova TS (2017) Effect of annealing on the microstructure and mechanical properties of ultrafine-grained commercially pure Al. *Phys Solid State* 59(10):1970–1977
- [21] An XH, Wu SD, Zhang ZF, Figueiredo RB, Gao N, Langdon TG (2012) Enhanced strength–ductility synergy in nanostructured Cu and Cu–Al alloys processed by high-pressure torsion and subsequent annealing. *Scr Mater* 66(5):227–230
- [22] Lin Y, Liu W, Wang L, Lavernia EJ (2013) Ultra-fine grained structure in Al–Mg induced by discontinuous dynamic recrystallization under moderate straining. *Mater Sci Eng A* 573:197–204
- [23] Sharma G, Ramanujan RV, Tiwar GP (2000) Instability mechanisms in lamellar microstructures. *Acta Mater* 48:875–889

- [24] Budiman AS, Li N, Wei Q, Baldwin JK, Xiong J, Luo H, Trugman D, Jia QX et al (2011) Growth and structural characterization of epitaxial Cu/Nb multilayers. *Thin Solid Films* 519(13):4137–4143
- [25] Sandim MJR, Sandim HRZ, Shigue CY, Filgueira M, Ghivelder L (2003) Annealing effects on the magnetic properties of a multifilamentary Cu–Nb composite. *Supercond Sci Technol* 16:307–313
- [26] Sallez N, Boulnat X, Borbély A, Béchade JL, Fabrègue D, Perez M, de Carlan Y, Hennet L et al (2015) In situ characterization of microstructural instabilities: recovery, recrystallization and abnormal growth in nanoreinforced steel powder. *Acta Mater* 87:377–389
- [27] Mara NA, Misra A, Hoagland RG, Sergueeva AV, Tamayo T, Dickerson P, Mukherjee AK (2008) High-temperature mechanical behavior/microstructure correlation of Cu/Nb nanoscale multilayers. *Mater Sci Eng A* 493(1–2):274–282
- [28] Zheng S, Carpenter JS, McCabe RJ, Beyerlein IJ, Mara NA (2014) Engineering interface structures and thermal stabilities via SPD processing in bulk nanostructured metals. *Sci Rep* 4:4226
- [29] Deng L, Han K, Wang B, Yang X, Liu Q (2015) Thermal stability of Cu–Nb microcomposite wires. *Acta Mater* 101:181–188
- [30] Schneider J, Cobb J, Carpenter JS, Mara NA (2018) Maintaining nano-lamellar microstructure in friction stir welding (FSW) of accumulative roll bonded (ARB) Cu–Nb nano-lamellar composites (NLC). *J Mater Sci Technol* 34(1):92–101
- [31] Sandim MJR, Shigue CY, Ribeiro LG, Filgueira M, Sandim HRZ (2002) Annealing effects on the electrical and superconducting properties of a Cu–15 vol%Nb composite conductor. *IEEE Trans Appl Supercond* 12:1195–1198
- [32] Misra A, Hoagland RG, Kung H (2004) Thermal stability of self-supported nanolayered Cu/Nb ribbons. *Philos Mag* 84:1021–1028
- [33] Hong SI, Hill MA (2000) Microstructural stability of Cu–Nb microcomposite wires fabricated by the bundling and drawing process. *Mater Sci Eng A* 281:189–197
- [34] Bouaziz O (2007) Embury JD (2007) Microstructural design for advance structural steels. *Mater Sci Forum* 42(539–543):42–50
- [35] Beyerlein IJ, Caro A, Demkowicz MJ, Mara NA, Misra A, Uberuaga BP (2013) Radiation damage tolerant nanomaterials. *Mater Today* 16(11):443–449
- [36] Beyerlein IJ, Mayeur JR (2015) Mesoscale investigations for the evolution of interfaces in plasticity. *Curr Opin Solid State Mater* 19(4):203–211
- [37] Beyerlein IJ, Mayeur JR, McCabe RJ, Zheng SJ, Carpenter JS, Mara NA (2014) Influence of slip and twinning on the crystallographic stability of bimetal interfaces in nanocomposites under deformation. *Acta Mater* 72:137–147
- [38] McCabe RJ, Carpenter JS, Vogel S, Mara NA, Beyerlein IJ (2015) Recrystallization and grain growth in accumulative roll-bonded metal composites. *JOM* 67(12):2810–2819
- [39] Zheng S, Carpenter JS, Wang J, Mara NA, Beyerlein IJ (2014) An interface facet driven Rayleigh instability in high-aspect-ratio bimetallic nanolayered composites. *Appl Phys Lett* 105(111901):1–5
- [40] Deng L, Han K, Hartwig KT, Siegrist TM, Dong L, Sun Z, Yang X, Liu Q (2014) Hardness, electrical resistivity, and modeling of in situ Cu–Nb microcomposites. *J Alloys Compd* 602:331–338
- [41] Dubois JB, Thilly L, Renault PO, Lecouturier F, Di Michiel M (2010) Thermal stability of nanocomposite metals: in situ observation of anomalous residual stress relaxation during annealing under synchrotron radiation. *Acta Mater* 58:6504–6512
- [42] Lewis AC, Josell D, Weihs TP (2003) Stability in thin ribbon multilayers and microlaminates: the role of free energy, structure, and orientation at interfaces and grain boundaries. *Scr Mater* 48:1079–1085
- [43] Wan H, Shen Y, Wang J, Shen Z, Jin X (2012) A predictive model for microstructure evolution in metallic multilayers with immiscible constituents. *Acta Mater* 60:6869–6881
- [44] Srinivasan D, Subramanian PR (2007) Kirkendall porosity during thermal treatment of Mo–Cu nanomultilayers. *Mater Sci Eng A* 459:145–150
- [45] Zheng S, Beyerlein IJ, Carpenter JS, Kang K, Wang J, Han W, Mara NA (2013) High-strength and thermally stable bulk nanolayered composites due to twin-induced interfaces. *Nat Commun* 2651:1–8
- [46] Thilly L, Lecouturier F, Von Stebut J (2002) Size-induced enhanced mechanical properties of nanocomposite copper/niobium wires: nanoindentation study. *Acta Mater* 50:5049–5065
- [47] Man O, Pantělejev L, Kunz L (2010) Study of thermal stability of ultrafine-grained copper by means of electron back scattering diffraction. *Mater Trans* 51:209–213
- [48] Gu CF, Davies CHJ (2010) Thermal stability of ultrafine-grained copper during high speed micro-extrusion. *Mater Sci Eng A* 527:1791–1799
- [49] Saldana C, King AH, Stach EA, Compton WD, Chandrasekar S (2011) Vacancies, twins, and the thermal stability of ultrafine-grained copper. *Appl Phys Lett* 99:231911–231913
- [50] Cao P, Zhang D (2006) Thermal stability of nanocrystalline copper ribbons. *Int J Mod Phys B* 20:3830–3835
- [51] Popova EN, Popov VV, Romanov EP, Pilyugin VP (2006) Thermal stability of nanocrystalline Nb produced by severe plastic deformation. *Phys Met Metall* 101:52–57

- [52] Popov VV, Popova EN, Stolbovsky AV, Pilyugin VP (2011) The structure of Nb obtained by severe plastic deformation and its thermal stability. *Mater Sci Forum* 667–669:409–414
- [53] Wang YL, Lapovok R, Wang JT, Qi YS, Estrin Y (2015) Thermal behavior of copper processed by ECAP with and without back pressure. *Mater Sci Eng A* 628:21–29
- [54] Ma H, Zou Y, Sologubenko AS, Spolenak R (2015) Copper thin ribbons by ion beam assisted deposition: strong texture, superior thermal stability and enhanced hardness. *Acta Mater* 98:17–28
- [55] Li BL, Goldfrey A, Liu Q (2004) Subdivision of original grains during cold-rolling of interstitial-free steel. *Scr Mater* 50:879–883
- [56] Field DP, Bradford LT, Nowell MM, Lillo TM (2007) The role of annealing twins during recrystallization of Cu. *Acta Mater* 55:4233–4241
- [57] El-Dasher BS, Adams BL, Rollett AD (2003) Viewpoint: experimental recovery of geometrically necessary dislocation density in polycrystals. *Scr Mater* 48:141
- [58] Dupouy F, Snoeck E, Casanove MJ, Roucau C, Peyrade JP, Askenazy S (1996) Microstructural characterization of high strength and high conductivity nanocomposite wires. *Scr Mater* 34(7):1067
- [59] Snoeck E, Lecouturier F, Thilly L, Casanove MJ, Rakoto H, Coffe G, Askenazy S, Peyrade JP et al (1998) Microstructural studies of in Situ produced filamentary Cu/Nb wires. *Scr Mater* 38(11):1643–1648
- [60] Leprince-Wang Y, Han K, Huang Y, Yu-Zhang K (2003) Microstructure in Cu–Nb microcomposites. *Mater Sci Eng A* 351(1–2):214–223
- [61] Lubensky TC, Socolar JES, Steinhardt PJ, Bancel PA, Heiney PA (1986) Distortion and peak broadening in quasicrystal diffraction patterns. *Phys Rev Lett* 57:1440–1443
- [62] Bobylev SV, Ovid'ko IA (2017) Stress-driven migration, convergence and splitting transformations of grain boundaries in nanomaterials. *Acta Mater* 124:333–342
- [63] Lei R, Wang M, Wang H, Xu S (2016) New insights on the formation of supersaturated Cu–Nb solid solution prepared by mechanical alloying. *Mater Charact* 118:324–331
- [64] Humphreys FJ, Hatherly M (2004) Recrystallization and related annealing phenomena, 2nd edn. Elsevier, Oxford
- [65] Lian J, Valiev RZ, Baudalet B (1995) On the enhanced grain growth in ultrafine grained metals. *Acta Metall Mater* 43:4165–4170
- [66] Winning M, Gottstein G, Shvindlerman LS (2002) On the mechanisms of grain boundary migration. *Acta Mater* 50:353–363
- [67] De Knijf D, Santofimia MJ, Shi H, Bliznuk V, Föjér C, Petrov R, Xu W (2015) In situ austenite–martensite interface mobility study during annealing. *Acta Mater* 90:161–168
- [68] Raabe D, Ohsaki S, Hono K (2009) Mechanical alloying and amorphization in Cu–Nb–Ag in situ composite wires studied by transmission electron microscopy and atom probe tomography. *Acta Mater* 57:5254–5263
- [69] Voorhees PW (1992) Ostwald ripening of two-phase mixtures. *Annu Rev Mater Sci* 22:197–215
- [70] Deng LP, Wang BS, Xiang HL, Yang XF, Niu RM, Han K (2016) Effect of annealing on the microstructure and properties of in situ Cu–Nb microcomposite wires. *Acta Metall Sin (Engl Lett)* 29:668–673